

Y5F3[AsO3]4 and Y5Cl3[AsO3]4: two non-isostructural yttrium halide oxoarsenates(III) and their potential as hosts for luminescent Eu³⁺- and Tb³⁺-doping



Ralf J. C. Locke, Martina Mikuta, Florian Ledderboge, Frank C. Zimmer, Henning A. Höppe, Thomas Schleid

Angaben zur Veröffentlichung / Publication details:

Locke, Ralf J. C., Martina Mikuta, Florian Ledderboge, Frank C. Zimmer, Henning A. Höppe, and Thomas Schleid. 2025. "Y5F3[AsO3]4 and Y5Cl3[AsO3]4: two non-isostructural yttrium halide oxoarsenates(III) and their potential as hosts for luminescent Eu³⁺- and Tb³⁺-doping." *Crystals* 15 (7): 611. <https://doi.org/10.3390/cryst15070611>.

Article

Y₅F₃[AsO₃]₄ and Y₅Cl₃[AsO₃]₄: Two Non-Isostructural Yttrium Halide Oxoarsenates(III) and Their Potential as Hosts for Luminescent Eu³⁺- and Tb³⁺-Doping

Ralf J. C. Locke¹, Martina Mikuta², Florian Ledderboge¹, Frank C. Zimmer¹, Henning A. Höpfe² 
and Thomas Schleid^{1,*} 

¹ Institut für Anorganische Chemie, Universität Stuttgart, Pfaffenwaldring 55, 70569 Stuttgart, Germany

² Institut für Physik, Universität Augsburg, Universitätsstraße 1, 86159 Augsburg, Germany

* Correspondence: schleid@iac.uni-stuttgart.de

Abstract

Y₅F₃[AsO₃]₄ crystallizes needle-shaped in the tetragonal space group *P4/ncc* with the lattice parameters *a* = 1143.80(8) pm, *c* = 1078.41(7) pm and *c/a* = 0.9428 for *Z* = 4. The yttrium-fluoride substructure linked via secondary contacts forms a three-dimensional network $\infty_3\{[Y_5F_3]^{12+}\}$ and the remaining part consists of ψ^1 -tetrahedral [AsO₃]³⁻ units, which leave lone-pair channels along [001]. In contrast, platelet-shaped Y₅Cl₃[AsO₃]₄ crystals adopt the monoclinic space group *C2/c* with the lattice parameters *a* = 1860.56(9) pm, *b* = 536.27(3) pm, *c* = 1639.04(8) pm and β = 105.739(3)° for *Z* = 4. Condensation of [(Y_{1,2})O₈]¹³⁻ polyhedra via four common edges each leads to fluorite-like $\infty_2\{[(Y_{1,2})O_e^{8/2}]^{5-}\}$ layers spreading out parallel to the (100) plane. Their three-dimensional linkage occurs via the (Y₃)³⁺ cations with their Cl⁻ ligands on the one hand and the As³⁺ cations with their lone-pairs of electrons on the other, which also form within [AsO₃]³⁻ anions lone-pair channels along [010]. Both colorless compounds can be obtained by solid-state reactions from corresponding mixtures of the binaries (Y₂O₃, As₂O₃ and YX₃ with X = F and Cl) at elevated temperatures of 825 °C, most advantageously under halide-flux assistance (CsBr for Y₅F₃[AsO₃]₄ and ZnCl₂ for Y₅Cl₃[AsO₃]₄). By replacing a few percent of YX₃ with EuX₃ or TbX₃, Eu³⁺- or Tb³⁺-doped samples are accessible, which show red or green luminescence upon excitation with ultraviolet radiation.

Keywords: yttrium; halides; oxoarsenates(III); crystal structures; luminescence



Academic Editor: Kil Sik Min

Received: 28 May 2025

Revised: 27 June 2025

Accepted: 27 June 2025

Published: 30 June 2025

Citation: Locke, R.J.C.; Mikuta, M.; Ledderboge, F.; Zimmer, F.C.; Höpfe, H.A.; Schleid, T. Y₅F₃[AsO₃]₄ and Y₅Cl₃[AsO₃]₄: Two Non-Isostructural Yttrium Halide Oxoarsenates(III) and Their Potential as Hosts for Luminescent Eu³⁺- and Tb³⁺-Doping. *Crystals* **2025**, *15*, 611. <https://doi.org/10.3390/cryst15070611>

Copyright: © 2025 by the authors. Licensee MDPI, Basel, Switzerland. This article is an open access article distributed under the terms and conditions of the Creative Commons Attribution (CC BY) license (<https://creativecommons.org/licenses/by/4.0/>).

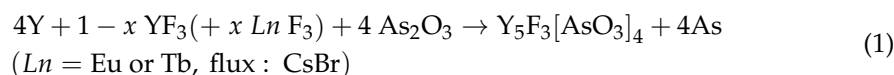
1. Introduction

As a consequence of the lanthanoid contraction, yttrium displays a cationic radius ($r_i(Y^{3+}) = 101.9$ pm, *Z*(Y) = 39) close to the one of holmium ($r_i(Ho^{3+}) = 101.5$ pm, *Z*(Ho) = 67), despite having only half the atomic mass [1]. Owing to the electronic closed-shell situation of Y³⁺ ([Kr]), yttrium(III) compounds serve as perfect hosts for getting doped with same-size luminescent cations of the lanthanoid series (e.g., Eu³⁺ or Tb³⁺), especially when they contain hard anions (O²⁻ or F⁻) to avoid quenching effects. But not only Y₂O₃ [2] and YF₃ [3] are suitable for this purpose, also mixed anionic compounds like YOF [4] are promising candidates, even when they bear soft anions (e.g., YOCl [5] or Y₂O₂S [6]). Moreover, the necessary energy-transfer processes for luminescence can be eased, when inorganic antennae are present in more complex systems, such as fluoride salts with oxoanions. These serve as energy reservoirs for incoming radiation and act with charge-transfer

or electronic lone-pair activities. Most prominent examples are the oxomolybdates(VI) and oxotungstates(VI) $\text{YF}[\text{MoO}_4]$ [7] and $\text{YF}[\text{WO}_4]$ [8] for the first, or the oxoselenates(IV) $\text{YF}[\text{SeO}_3]$ [9,10] and $\text{Y}_3\text{F}[\text{SeO}_3]_4$ [11] for the second case. Even here, the softer Cl^- anions can be tolerated, as the chloride oxomolybdate(VI) $\text{YCl}[\text{MoO}_4]$ [7], the chloride oxotungstate(VI) $\text{YCl}[\text{WO}_4]$ [12,13] and the chloride oxoantimonate(III) YClSb_2O_4 [14] might demonstrate. The idea of combining most of these prerequisites leads to investigations of the yttrium(III) halide oxoarsenates(III) $\text{Y}_5\text{X}_3[\text{AsO}_3]_4$ ($\text{X} = \text{F}$ and Cl) as host materials for doping with small amounts of Eu^{3+} or Tb^{3+} in order to harvest red or green light from a colorless compound upon UV irradiation.

2. Experimental

The new yttrium(III) fluoride oxoarsenate(III) $\text{Y}_5\text{F}_3[\text{AsO}_3]_4$ and its doped samples could be prepared via partial metallothermic reduction. For this purpose, elemental yttrium (Y: ChemPur, 99.9%, 89.5 mg), yttrium trifluoride (YF_3 : Heraeus, 99.9%, 35.6 mg) and arsenic sesquioxide (As_2O_3 : Aldrich, 99.99%, 199.2 mg) were reacted within a flux of cesium bromide (CsBr: Merck, 99.9%, 800 mg) in evacuated glassy silica ampoules (Equation (1)). Europium trifluoride (EuF_3 : ChemPur, 99.9%, 1.6 mg) and terbium trifluoride (TbF_3 : ChemPur, 99.9%, 1.6 mg) were used as dopants, replacing aliquots of YF_3 .



The ampoules were sealed under inert gas (argon), treated with a temperature program at 825 °C and brought to room temperature over several days. In this way, phase-pure powders could be obtained and only the monolithically grown single crystal of arsenic per batch had to be removed. As an example, Figure 1 shows the *Rietveld* refinement of an undoped powder sample of $\text{Y}_5\text{F}_3[\text{AsO}_3]_4$ measured with a STADI-P diffractometer (Stoe & Cie, Darmstadt, Germany) using $\text{Cu-K}\alpha$ radiation ($\lambda = 154.06$ pm).

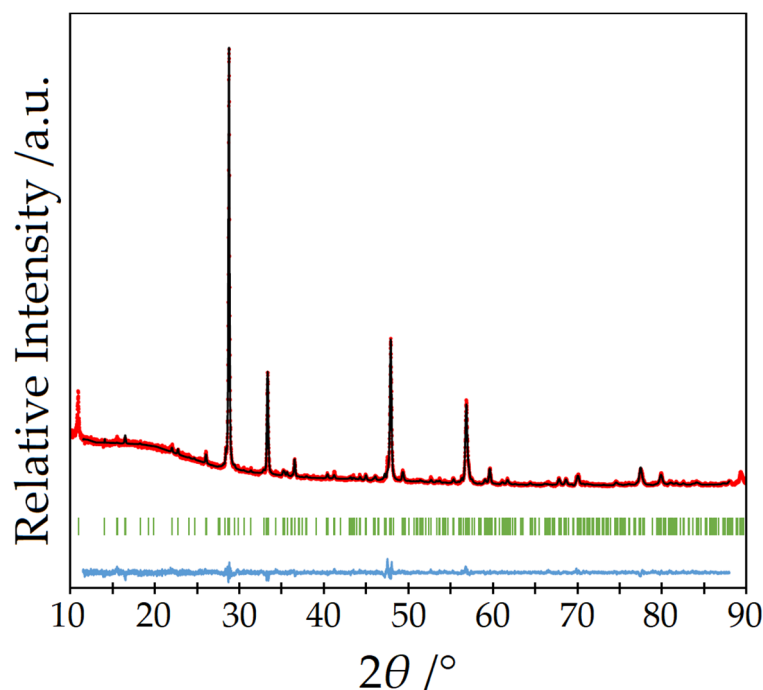
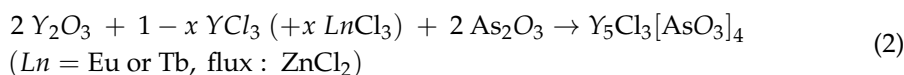


Figure 1. *Rietveld* refinement (black) of a powder diffractogram of undoped $\text{Y}_5\text{F}_3[\text{AsO}_3]_4$ (red) with the Bragg positions (green) of $\text{Y}_5\text{F}_3[\text{AsO}_3]_4$ and the $Y_{\text{obs}} - Y_{\text{cal}}$ difference curve (blue).

The new yttrium(III) chloride oxoarsenate(III) $Y_5Cl_3[AsO_3]_4$ and its doped samples were able to be prepared by mixing yttrium sesquioxide (Y_2O_3 : Merck, 99.99%, 108.3 mg), yttrium trichloride (YCl_3 : ChemPur, 99.9%, 45.4 mg) and arsenic sesquioxide (As_2O_3 : Aldrich, 99.99%, 94.9 mg) with a flux of zinc chloride ($ZnCl_2$: Merck, 99.9%, 800 mg) in evacuated glassy silica ampoules (Equation (2)). Europium trichloride ($EuCl_3$: Aldrich, 99.9%, 1.9 mg) and terbium trichloride ($TbCl_3$: ChemPur, 99.9%, 1.9 mg) were used as dopants to replace the corresponding amounts of YCl_3 .



The ampoules were sealed under inert gas (argon), treated with a temperature program at 825 °C and brought to room temperature over several days. In this way, also phase-pure powder samples could be obtained. As an example, Figure 2 shows the *Rietveld* refinement of an undoped powder of $Y_5Cl_3[AsO_3]_4$ measured with a Rigaku SmartLab X-ray powder diffractometer (Rigaku, Tokyo, Japan) with $Cu-K\alpha$ radiation ($\lambda = 154.06$ pm).

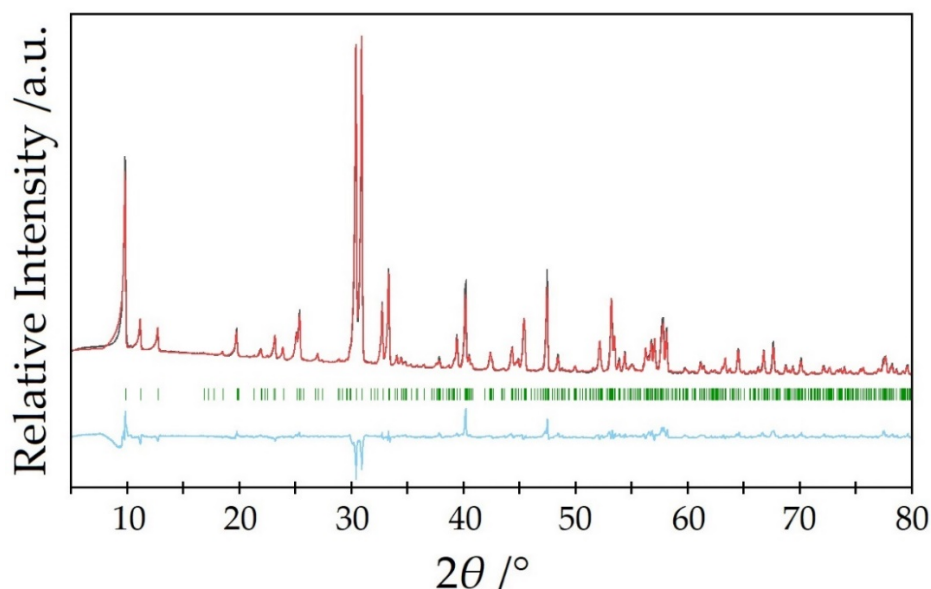


Figure 2. *Rietveld* refinement (black) of a powder diffractogram of undoped $Y_5Cl_3[AsO_3]_4$ (red) with the Bragg positions (green) of $Y_5Cl_3[AsO_3]_4$ and the $Y_{obs} - Y_{cal}$ difference curve (blue).

Suitable single crystals of needle-shaped $Y_5F_3[AsO_3]_4$ and platelet-shaped $Y_5Cl_3[AsO_3]_4$ (Figure 3) were transferred into glass capillaries (Hilgenberg, Malsfeld, Germany) and fixed with grease, then measured with $Mo-K\alpha$ radiation ($\lambda = 71.07$ pm) on a κ -CCD single-crystal diffractometer (Bruker-Nonius, Karlsruhe, Germany). After numerical absorption correction with the program HABITUS, included in the X-SHAPE [15] suite, using the SHELX-97 program package [16], the resulting data sets could be solved and successfully refined with direct methods in the tetragonal space group $P4/ncc$ for $Y_5F_3[AsO_3]_4$ and in the monoclinic space group $C2/c$ for $Y_5Cl_3[AsO_3]_4$.

The samples were recorded on an FS920 fluorescence spectrometer (Edinburgh Instruments, Livingston, UK) at room temperature with a Xe900 continuous xenon lamp. Three scans were recorded with respect to the lamp intensity and the average is displayed in the spectra. They were plotted and standardized with respect to their intensity with Origin 2019b.

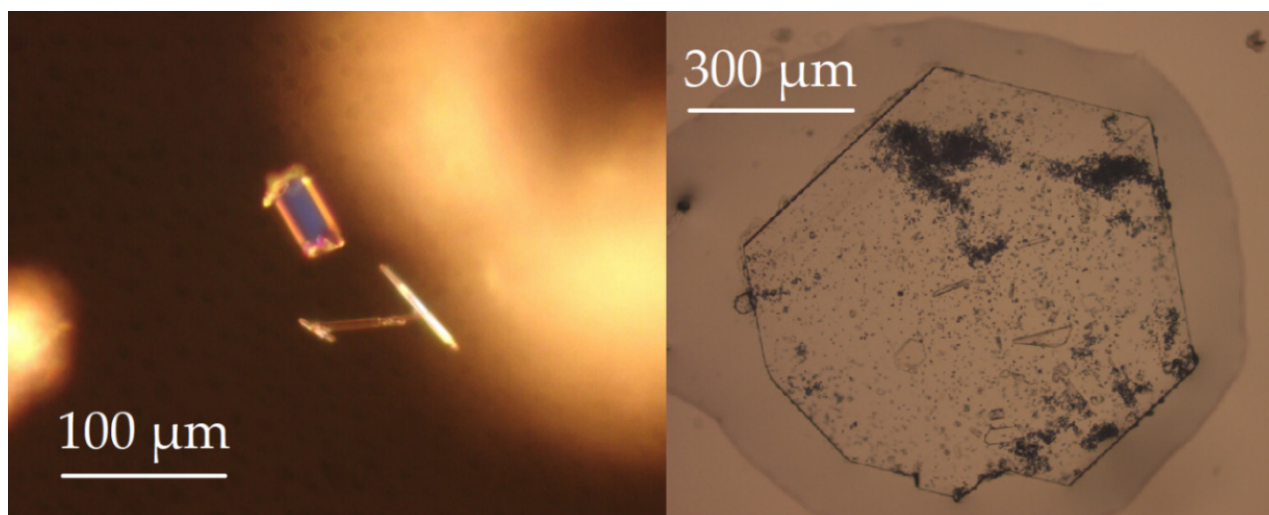


Figure 3. Brick- or needle-shaped crystals of $Y_5F_3[AsO_3]_4$ (left) and platelet-shaped crystal of $Y_5Cl_3[AsO_3]_4$ (right).

3. Results and Discussion

3.1. Crystal-Structure Description of $Y_5F_3[AsO_3]_4$

The new yttrium(III) fluoride oxoarsenate(III) $Y_5F_3[AsO_3]_4$ crystallizes needle-shaped in the tetragonal space group $P4/ncc$ with the lattice parameters $a = 1143.80(8)$ pm, $c = 1078.41(7)$ pm and $c/a = 0.943$ for $Z = 4$. As expected and as can be seen from the Shannon radii [1], it should assume a unit-cell size between those of $Dy_5F_3[AsO_3]_4$ ($a = 1148.34(8)$ pm, $c = 1082.69(7)$ pm, $c/a = 0.943$) [17] and $Ho_5F_3[AsO_3]_4$ ($a = 1143.26(8)$ pm, $c = 1078.14(7)$ pm, $c/a = 0.943$) [17] in terms of the unit-cell dimensions.

There are three different cationic sites present in this structure, two of them belong to yttrium (4c for Y1 and 16g for Y2) and one to arsenic (16g). In contrast, the anions have five different sites, three of which belong to oxygen (all at 16g) and two to fluorine (4c for F1 and 8f for F2). The $(Y1)^{3+}$ cation centers a square prism of oxygen ($d(Y1-O) = 243-249$ pm), which is capped by two fluoride anions $[(Y1)O_8(F1)(F1')]^{15-}$. One F^- anion comes close to $(Y1)^{3+}$ ($d(Y1-F1) = 240$ pm), while the second one is much further away ($d(Y1 \cdots F1') = 300$ pm) and can therefore only be regarded as a secondary-contact ligand (Figure 4, left). In contrast, the $(Y2)^{3+}$ cation forms a bicapped trigonal prism $[(Y2)O_6F_2]^{11-}$ with six oxygen atoms and two fluoride anions without secondary contacts (Figure 4, mid). However, the range of bond lengths is significantly wider ($d(Y2-F) = 221-261$ pm, $d(Y2-O) = 227-250$ pm). These distances are still within the expected range, however, especially when compared with $Y_7O_6F_9$ [18,19], where yttrium-fluorine distances from 218 to 260 pm (plus 300 pm) are present and secondary contacts occur here as well. The yttrium-oxygen distances of 220–268 pm also fall into a similar interval. The As^{3+} cation forms an isolated ψ^1 -tetrahedron $[AsO_3]^{3-}$ with three oxygen atoms (Figure 4, right), showing arsenic-oxygen distances in the range from 176 to 181 pm, which are quite typical, especially when compared with the crystalline As_2O_3 modifications (claudetite-I: 172–181 pm [20], claudetite-II: 177–182 pm [21], arsenolite: ~179 pm [22]).

The structure becomes easier to understand, if it is divided into two units, firstly the ψ^1 -tetrahedron $[AsO_3]^{3-}$ as just presented, and secondly the substructure of fluoride and yttrium. Both fluoride anions have clearly very different coordination environments. While $(F1)^-$ is surrounded by five plus one Y^{3+} cations in the shape of an elongated octahedron $[(F1)(Y2)_4(Y1)(Y1')]^{17+}$, $(F2)^-$ forms a chevron $[(F2)(Y2)_2]^{5+}$ ($\angle(Y2-F2-Y2) = 147^\circ$) with just two Y^{3+} cations (Figure 5).

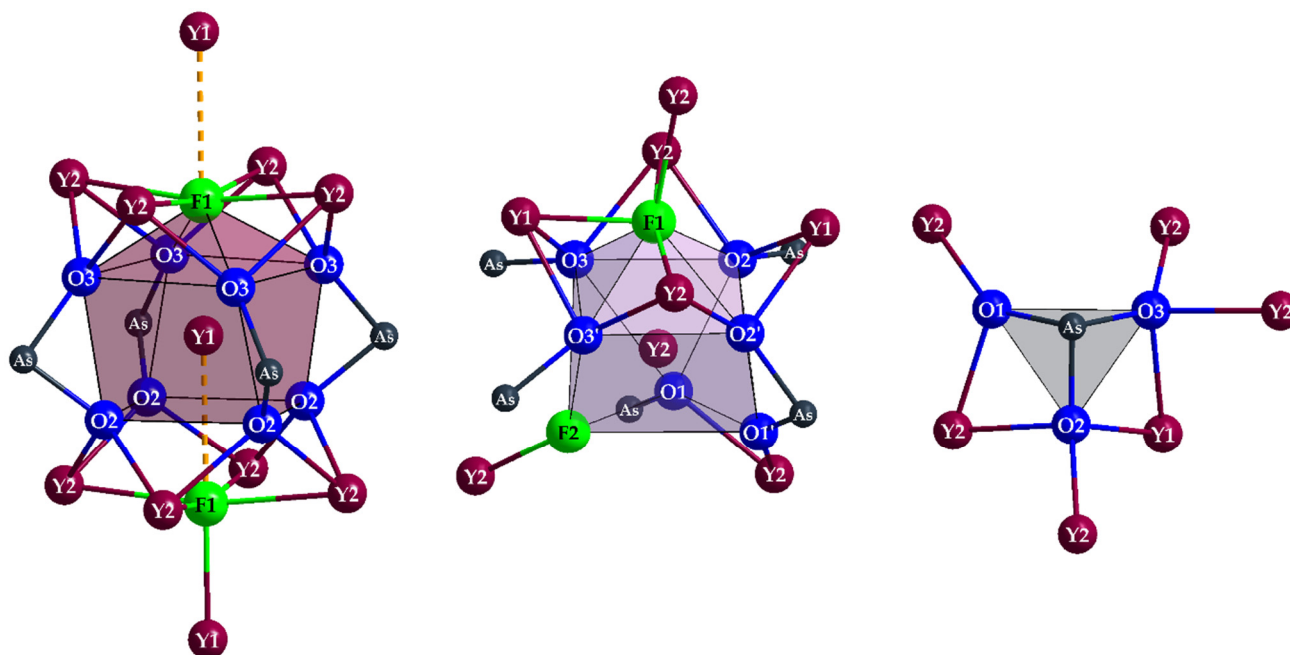


Figure 4. Capped square prism $[(Y1)O_8(F1)(F1')]^{15-}$ (left), bicapped trigonal prism $[(Y2)O_6F_2]^{11-}$ (mid) and ψ^1 -tetrahedron $[AsO_3]^{3-}$ (right) with complete cationic decoration in the tetragonal crystal structure of $Y_5F_3[AsO_3]$.

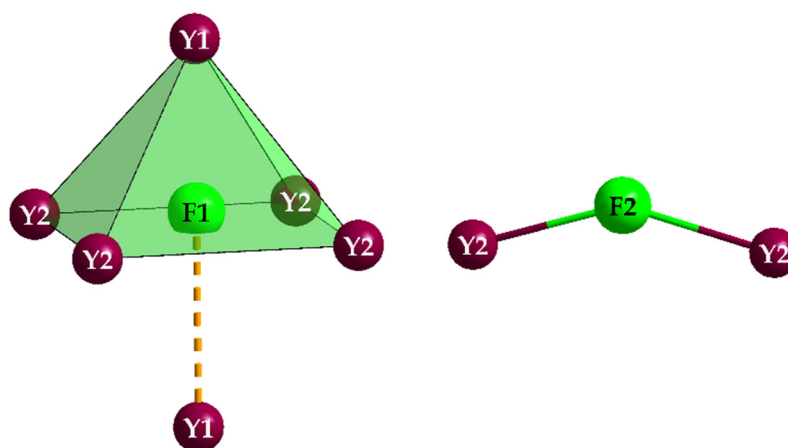


Figure 5. Capped square pyramid $[(F1)(Y2)_4(Y1)(Y1')]^{17+}$ (left) and chevron $[(F2)(Y2)_2]^{5+}$ (right) in the crystal structure of $Y_5F_3[AsO_3]_4$.

The $[(F1)(Y2)_4(Y1)(Y1')]^{17+}$ pseudo-octahedra form chains according to $\frac{1}{\infty} \{[(F1)(Y2)_{4/1}^t (Y1)_{2/2}^v]^{14+}\}$ (t = terminal, v = vertex-connecting) through corner-linkage via Y1, which run parallel to the c -axis. These chains are connected to the $[(F2)(Y2)_2]^{5+}$ chevrons via Y2 to create a three-dimensional network (Figure 6, top).

Figure 7 shows the combination of both substructures ($\frac{3}{\infty} \{[Y_5F_3]^{12+}\} + 4 [AsO_3]^{3-}$) with a view along $[001]$ and the unit-cell edges marked.

Table 1 summarizes the crystallographic data for $Y_5F_3[AsO_3]_4$, while Table 2 lists the atomic positions, Table 3 offers selected interatomic distances and Table 4 contains the motifs of mutual adjunction for its crystal structure.

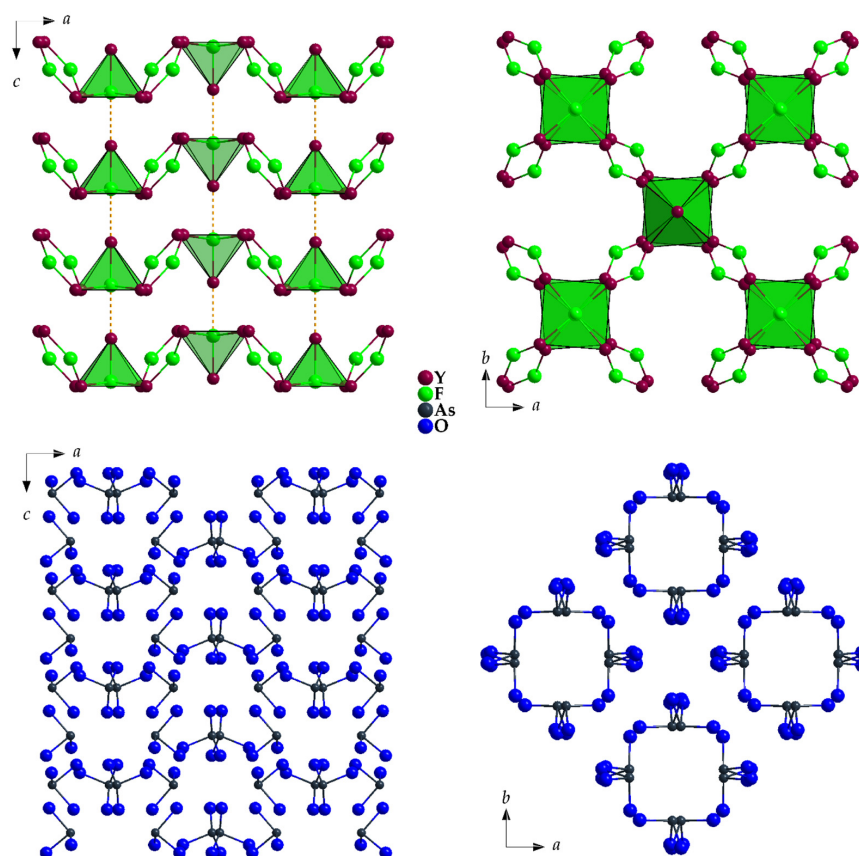


Figure 6. The yttrium-fluoride substructure linked via secondary $Y \cdots F'$ contacts to form a three-dimensional network $\infty^3 \{[Y_5F_3]^{12+}\}$ (top) and the substructure of ψ^1 -tetrahedral $[AsO_3]^{3-}$ anions, which leave channels along $[001]$ due to their lone pairs (bottom) in the crystal structure of $Y_5F_3[AsO_3]_4$ as viewed along $[010]$ (left) and $[001]$ (right).

Table 1. Crystallographic data of $Y_5F_3[AsO_3]_4$ and their determination.

Structured Formula		$Y_5F_3[AsO_3]_4$
Crystal system		tetragonal
Space group		$P4/ncc$ (no. 130)
Lattice parameters,	a/pm	1143.80(8)
	c/pm	1078.41(7)
	c/a	0.943
Number of formula units, Z		4
Calculated density, $D_x/\text{g}\cdot\text{cm}^{-3}$		4.676
Molar volume, $V_m/\text{cm}^3\cdot\text{mol}^{-1}$		212.41
Index range, $\pm h_{\max}, \pm k_{\max}, \pm l_{\max}$		14, 14, 13
Diffractometer limit, $2\theta/^\circ$		54.9
Electron sum, $F(000)/e^-$		1800
Absorption coefficient, μ/mm^{-1}		29.75
Extinction coefficient, ϵ/pm^{-3}		0.00106(7)
Measured reflections		20547
Independent ones		810
R_{int}/R_σ		0.096/0.041
Reflections with $ Fo \geq 4\sigma(Fo)$		620
R_1/R_1 with $ Fo \geq 4\sigma(Fo)$		0.056/0.034
wR_2/Goof		0.067/1.082
Residual electron density, $\rho_{\max/\min}/e^- \cdot 10^{-6} \text{pm}^{-3}$		0.80/−0.85
CSD number		2321105

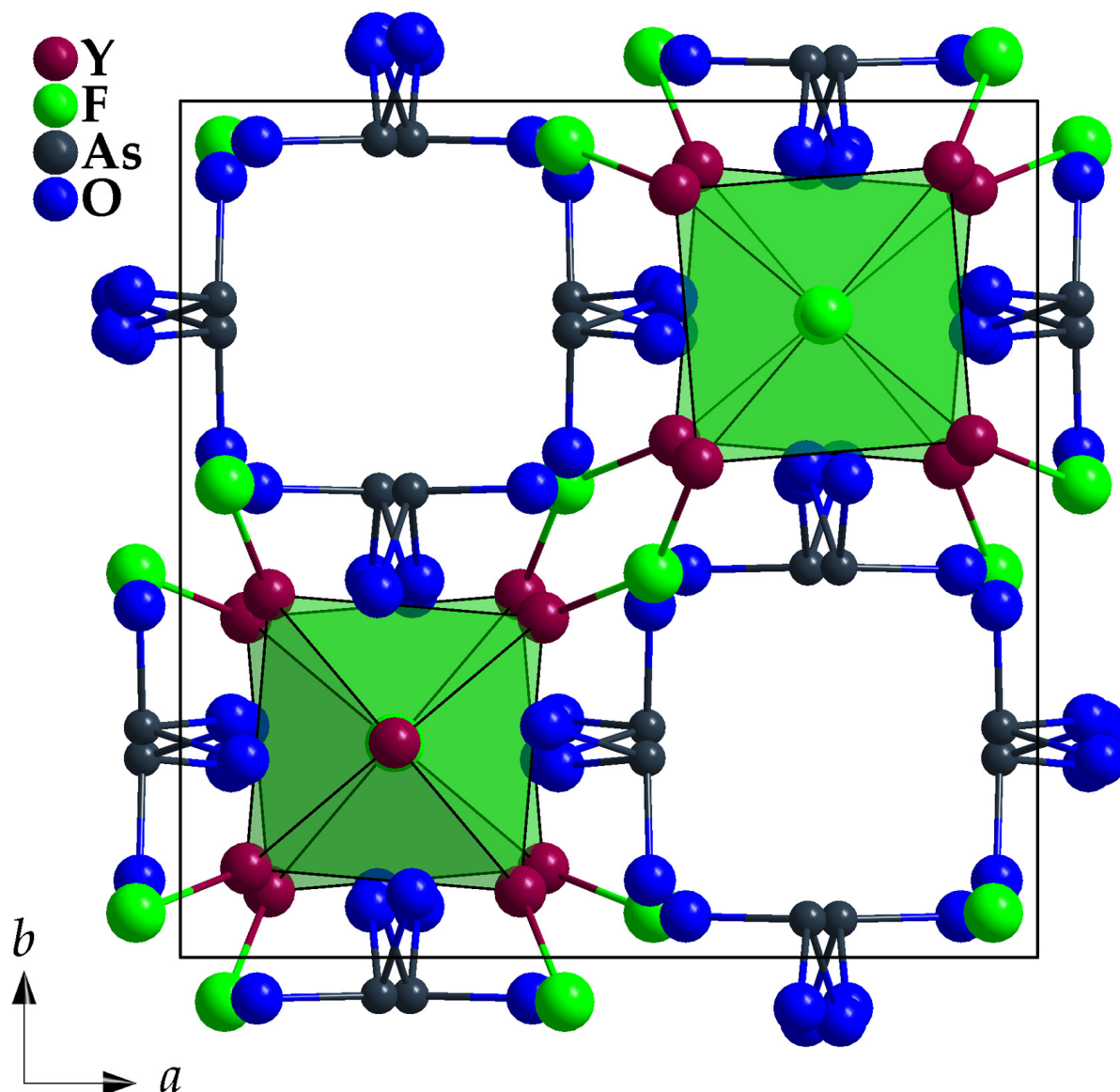


Figure 7. View at the unit-cell content of $\text{Y}_5\text{F}_3[\text{AsO}_3]_4$ along $[001]$ with emphasized vertex-connected $[\text{FY}_{5+1}]^{17+}$ polyhedra and discrete ψ^1 -tetrahedral $[\text{AsO}_3]^{3-}$ units.

Table 2. Fractional atomic coordinates, *Wyckoff* sites and symmetries as well as U_{eq} values for $\text{Y}_5\text{F}_3[\text{AsO}_3]_4$.

Atom	Site	x/a	y/b	z/c	$U_{\text{eq}}/\text{pm}^2$
Y1	4c	$1/4$	$1/4$	0.35328(11)	134(3)
Y2	16g	0.10339(5)	0.07674(5)	0.10733(6)	130(2)
F1	4c	$1/4$	$1/4$	0.1312(7)	172(16)
F2	8f	0.0517(4)	0.9483(4)	$1/4$	214(13)
As	16g	0.23168(6)	0.54424(6)	0.37332(7)	147(2)
O1	16g	0.0894(4)	0.5477(4)	0.4353(4)	190(11)
O2	16g	0.2702(4)	0.4265(4)	0.4764(4)	131(10)
O3	16g	0.2223(4)	0.4409(4)	0.2465(4)	167(11)

Table 3. Selected interatomic distances (d/pm) in the crystal structure of $\text{Y}_5\text{F}_3[\text{AsO}_3]_4$.

$[(\text{Y}1)\text{F}_{(1+1)}\text{O}_8]^{15-}$ polyhedron			
Y1–F1	(1×)		239.5(7)
Y1–O2	(4×)		242.8(4)
Y1–O3	(4×)		248.9(5)
Y1···F1	(1×)		299.7(7)
$[(\text{Y}2)\text{F}_2\text{O}_6]^{11-}$ polyhedron			
Y2–F2	(1×)		220.8(2)
Y2–O2	(1×)		227.4(4)
Y2–O1	(1×)		227.7(5)
Y2–O3	(1×)		229.8(4)
Y2–O1'	(1×)		234.3(4)
Y2–O2'	(1×)		237.4(4)
Y2–O3'	(1×)		250.4(4)
Y2–F1	(1×)		260.9(1)
$[\text{AsO}_3]^{3-}$ ψ^1-tetrahedron			
As–O1	(1×)		176.0(5)
As–O2	(1×)		180.1(4)
As–O3	(1×)		181.1(4)
$(\text{F}1)\text{Y}_{5+1}]^{17+}$ capped pyramid			
F1–Y1	(1×)		239.5(7)
F1–Y2	(4×)		260.9(1)
F1–Y1'	(1×)		299.7(7)
$(\text{F}2)\text{Y}_2]^{5+}$ chevron			
F2–Y2	(2×)		220.8(2)

Table 4. Motifs of mutual adjunction for the $\text{Y}_5\text{F}_3[\text{AsO}_3]_4$ structure.

	O1	O2	O3	F1	F2	C.N.
Y1	0/0	4/1	4/1	$1 + 1/1 + 1$	0/0	9 + 1
Y2	2/2	2/2	2/2	1/4	1/2	8
As	1/1	1/1	1/1	0/0	0/0	3
C.N.	3	4	4	5 + 1	2	

3.2. Crystal-Structure Description of $\text{Y}_5\text{Cl}_3[\text{AsO}_3]_4$

In spite of their identical crystallographic prerequisites (crystal system: monoclinic, space group: $C2/c$, Pearson symbol: mC96, Wyckoff sequence: $f^{11}e^1c^1$), the crystal structure of $\text{Y}_5\text{Cl}_3[\text{AsO}_3]_4$ differs considerably from the one of $\text{La}_5\text{Cl}_3[\text{AsO}_3]_4$ [23]. This is clearly reflected by their lattice parameters ($\text{Y}_5\text{Cl}_3[\text{AsO}_3]_4$: $a = 1860.56(9)$ pm, $b = 536.27(3)$ pm, $c = 1639.04(8)$ pm, $\beta = 105.739(3)^\circ$ versus $\text{La}_5\text{Cl}_3[\text{AsO}_3]_4$: $a = 1803.65(9)$ pm, $b = 548.39(3)$ pm, $c = 1723.16(9)$ pm, $\beta = 107.432(3)^\circ$ [23]) already, displaying a larger a -axis and a smaller c -axis, while the b -axis and the β -angle develop as expected by replacing the bigger La^{3+} ($r_i = 116$ pm) with the smaller Y^{3+} cation ($r_i = 102$ pm). The molar volumes of $237.0 \text{ cm}^3 \cdot \text{mol}^{-1}$ for the yttrium juxtaposed to $244.8 \text{ cm}^3 \cdot \text{mol}^{-1}$ for the lanthanum compound establish the anticipated trend, however.

Common structural features are three crystallographically different RE^{3+} cations ($\text{RE} = \text{Y}$ and La), two of them decorated with only eight oxygen atoms $[(\text{RE}1,2)\text{O}_8]^{13-}$, the third one with four oxygen atoms and four chloride anions $[(\text{RE}3)\text{O}_4\text{Cl}_4]^{9-}$, providing square hemi- or antiprismatic coordination spheres (Figure 8, top). All independent

oxygen atoms (O1–O6) belong as ligands to As^{3+} cations (As1 and As2) to constitute two different, but very similar ψ^1 -tetrahedral $[\text{AsO}_3]^{3-}$ anions (Figure 9) with pronounced stereochemical lone-pair activity.

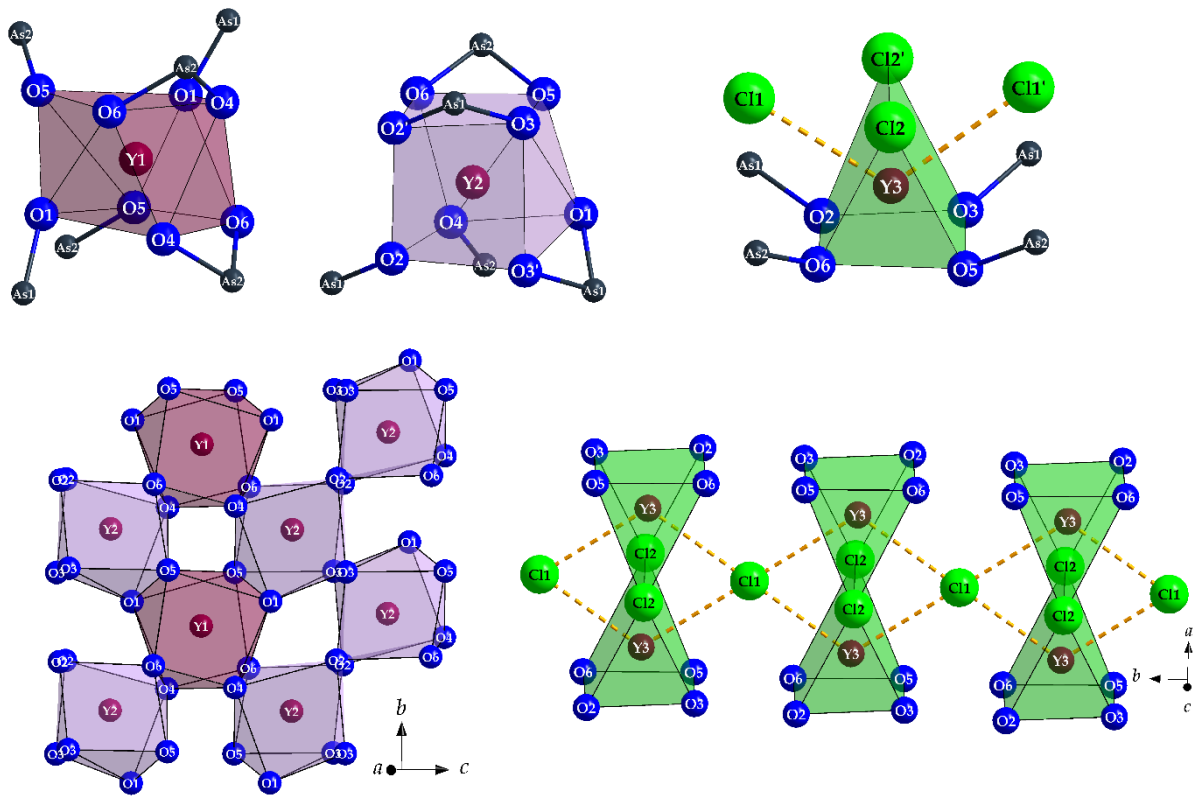


Figure 8. Square $[(\text{Y}1,2)\text{O}_8]^{13-}$ antiprism or prism and bicapped trigonal $[(\text{Y}3)\text{O}_4\text{Cl}_2\text{Cl}'_2]^{9-}$ prism in the crystal structure of $\text{Y}_5\text{Cl}_3[\text{AsO}_3]_4$ with their complete As^{3+} decoration (*top*) and their linkage via common oxygen edges to $\frac{2}{\infty} \{[(\text{Y}1,2)\text{O}_8]^{13-}\}$ layers parallel to the (100) plane (*bottom left*) and $\frac{2}{\infty} \{[(\text{Y}3)\text{O}_4\text{Cl}_2\text{Cl}'_2]^{9-}\}$ strands propagating along [010] (*bottom right*).

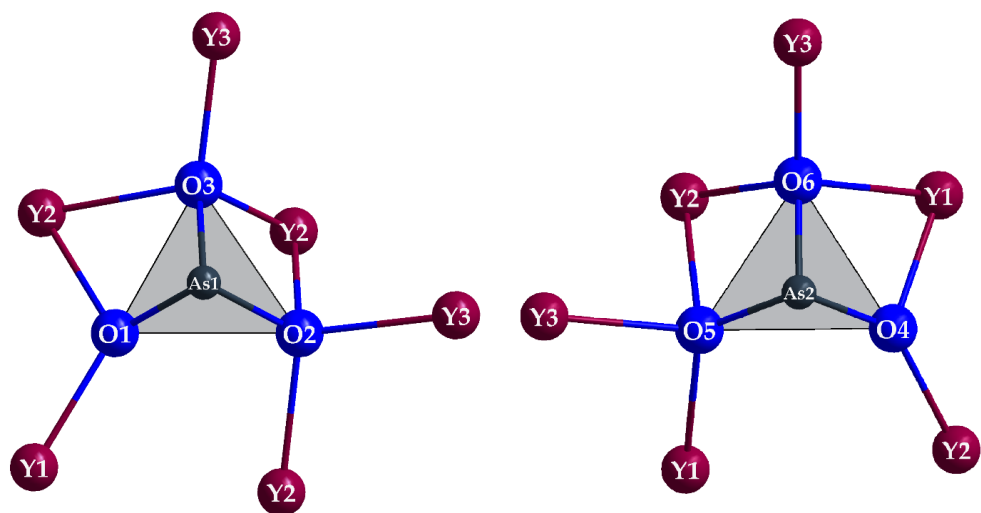


Figure 9. The two discrete ψ^1 -tetrahedral $[\text{AsO}_3]^{3-}$ anions in the crystal structure of $\text{Y}_5\text{Cl}_3[\text{AsO}_3]_4$ with their complete Y^{3+} decoration.

Remarkably different is the function of the two independent Cl^- anions, however. While Cl2 has two short contacts to Y3, Cl1 shows a peculiar coordination sphere of eight

almost equidistant trivalent cations (four Y^{3+} and four As^{3+}) arranged as an idealized cube (Figure 10). The other way around, $(Y3)^{3+}$ carries two close $(Cl2)^-$ and two far away $(Cl1)^-$ anions (Figure 8, right) as chloride ligands.

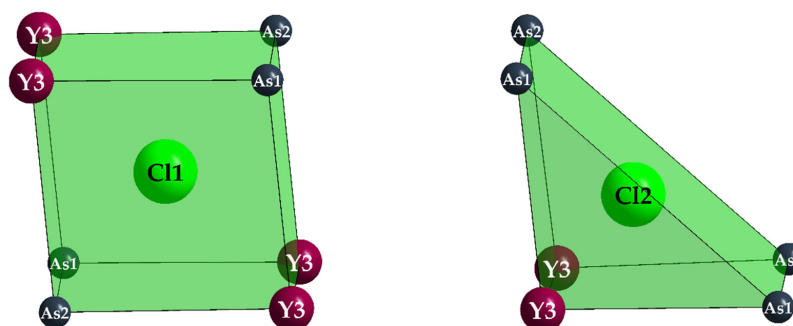


Figure 10. Square $[(Cl1)As_4Y_4]^{23+}$ (left) and trigonal $[(Cl2)As_4Y_2]^{17+}$ prism (right) in the crystal structure of $Y_5Cl_3[AsO_3]_4$.

Condensation of the $[(Y1)O_8]^{13-}$ and $[(Y2)O_8]^{13-}$ polyhedra via four common edges each leads to fluorite-like $\frac{2}{\infty} \{[(Y1,2)O_{8/2}]^e\}^{5-}$ (e = edge-connecting) layers spreading out parallel to the (100) plane (Figure 8, bottom left). Their three-dimensional linkage occurs via $(Y3)^{3+}$ cations with their Cl^- ligands as $\frac{2}{\infty} \{[(Y3)O_{4/1}(Cl2)_{2/2}(Cl1)_{2/4}]^v\}^{6.5-}$ (t = terminal, v = vertex-connecting) strands along [010] on the one hand (Figure 8, bottom right) and As^{3+} cations with their lone-pairs of electrons on the other (Figure 11).

Table 5 summarizes the crystallographic data for $Y_5Cl_3[AsO_3]_4$, while Table 6 lists the atomic positions, Table 7 offers selected interatomic distances and Table 8 contains the motifs of mutual adjunction for its crystal structure.

Table 5. Crystallographic data of $Y_5Cl_3[AsO_3]_4$ and their determination.

Structured Formula	$Y_5Cl_3[AsO_3]_4$
Crystal system	monoclinic
Space group	C2/c (no. 15)
a /pm	1860.56(9)
Lattice parameters, b /pm	536.27(3)
c /pm	1639.04(8)
β /°	105.739(3)
Number of formula units, Z	4
Calculated density, D_x /g·cm ⁻³	4.399
Molar volume, V_m /cm ³ ·mol ⁻¹	237.00
Index range, $\pm h_{max}, \pm k_{max}, \pm l_{max}$	24, 6, 20
Diffractometer limit, 2θ /°	55.0
Electron sum, $F(000)$ /e ⁻	1896
Absorption coefficient, μ /mm ⁻¹	27.14
Extinction coefficient, ϵ /pm ⁻³	0.00026(6)
Measured reflections	19174
Independent ones	1775
R_{int}/R_σ	0.115/0.077
Reflections with $ Fo \geq 4\sigma(Fo)$	1150
R_1/R_1 with $ Fo \geq 4\sigma(Fo)$	0.095/0.054
wR_2 /GooF	0.131/1.048
Residual electron density, $\rho_{max/min}$ /e ⁻ 10 ⁻⁶ pm ⁻³	1.83/-1.74
CSD number	2401390

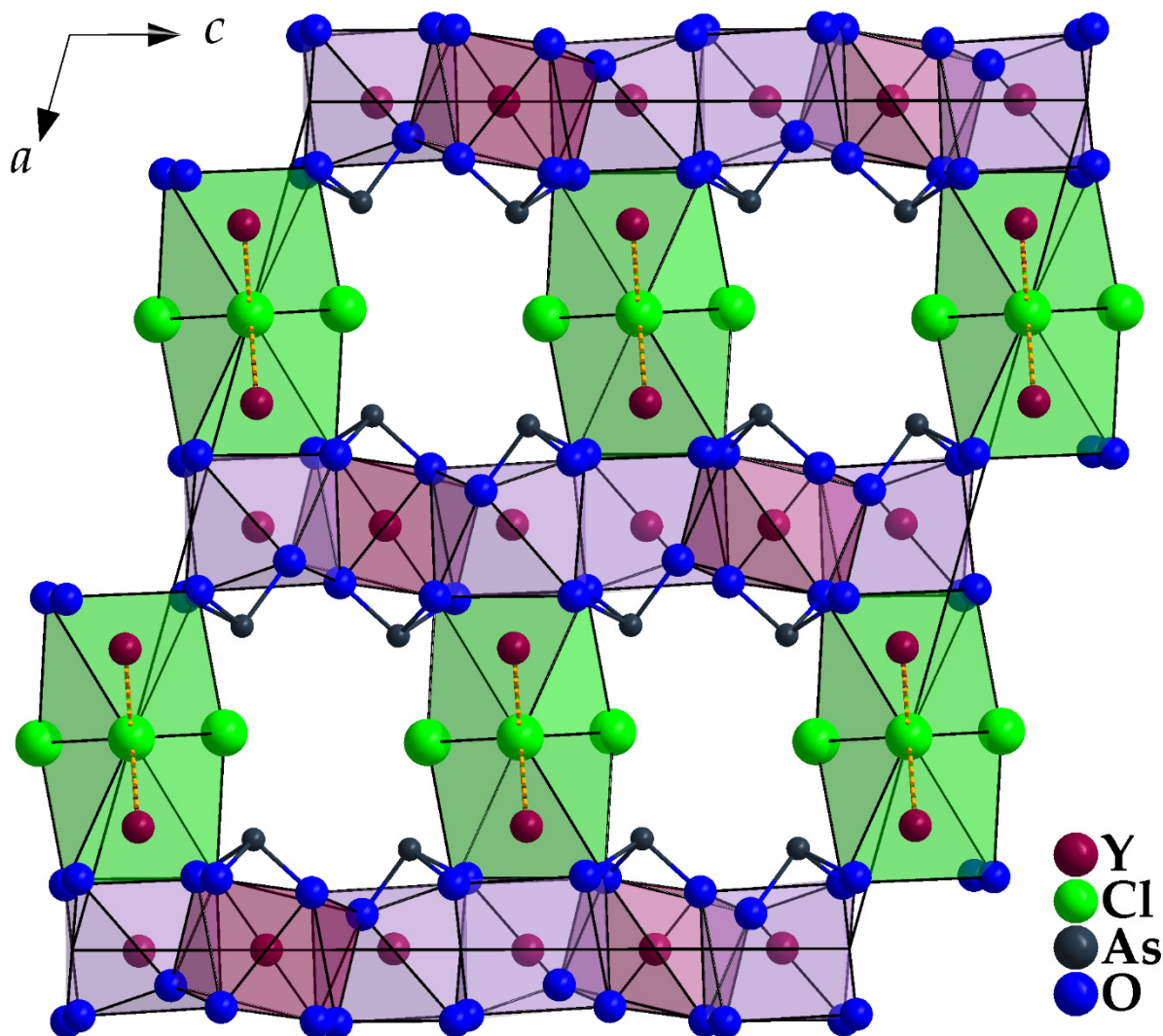


Figure 11. View at the unit-cell content of monoclinic $Y_5Cl_3[AsO_3]_4$ along $[010]$ with emphasized $[(Y1,2)O_8]^{13-}$ and $[(Y3)O_4Cl_2Cl'_2]^{9-}$ polyhedra and discrete ψ^1 -tetrahedral $[AsO_3]^{3-}$ units.

Table 6. Fractional atomic coordinates, *Wyckoff* sites and symmetries as well as U_{eq} values for $Y_5Cl_3[AsO_3]_4$.

Atom	Site	x/a	y/b	z/c	U_{eq}/pm^2
Y1	4e	0	0.1972(3)	$1/4$	158(4)
Y2	8f	0.49908(6)	0.2299(2)	0.41353(6)	168(3)
Y3	8f	0.14507(6)	0.2441(2)	0.45963(6)	198(3)
Cl1	4c	$1/4$	$1/4$	0	708(19)
Cl2	8f	0.25588(19)	0.2504(7)	0.3825(2)	402(8)
As1	8f	0.11822(6)	0.2590(2)	0.10200(7)	164(3)
O1	8f	0.0418(5)	0.3322(14)	0.1396(5)	268(20)
O2	8f	0.0772(4)	0.0079(13)	0.0325(4)	185(18)
O3	8f	0.0839(4)	0.4931(13)	0.0185(4)	173(18)
As2	8f	0.36980(6)	0.2556(2)	0.19349(7)	161(3)
O4	8f	0.4326(5)	0.3543(14)	0.2877(5)	226(19)
O5	8f	0.0844(5)	0.4989(13)	0.3399(4)	186(18)
O6	8f	0.4137(4)	0.4718(12)	0.1340(4)	165(18)

Table 7. Selected interatomic distances (d/pm) in the crystal structure of $\text{Y}_5\text{Cl}_3[\text{AsO}_3]_4$.

$[(\text{Y}1)\text{O}_8]^{13-}$ polyhedron			
2×	227.4(7)	Y1–O1	
2×	239.9(8)	Y1–O4	
2×	244.9(7)	Y1–O5	
2×	244.9(7)	Y1–O6	
$[(\text{Y}2)\text{O}_8]^{13-}$ polyhedron			
1×	220.1(7)	Y2–O4	
1×	232.6(7)	Y2–O3	
1×	235.1(7)	Y2–O1	
1×	236.8(7)	Y2–O6	
1×	238.8(7)	Y2–O2	
1×	248.4(8)	Y2–O3'	
1×	252.1(7)	Y2–O2'	
1×	255.9(8)	Y2–O5	
$[(\text{Y}3)\text{O}_4\text{Cl}_2\text{Cl}'_2]^{9-}$ polyhedron			
1×	218.4(7)	Y3–O6	
1×	219.3(7)	Y3–O3	
1×	238.0(8)	Y3–O2	
1×	240.7(7)	Y3–O5	
1×	269.5(4)	Y3–Cl2	
1×	273.9(3)	Y3–Cl2'	
1×	325.1(1)	Y3···Cl1	
1×	330.3(1)	Y3···Cl1'	
$[(\text{As}1)\text{O}_3]^{3-}$ ψ^1-tetrahedron			
1×	174.0(8)	As1–O1	
1×	179.5(8)	As1–O2	
1×	183.9(7)	As1–O3	
$[(\text{As}2)\text{O}_3]^{3-}$ ψ^1-tetrahedron			
1×	174.7(7)	As2–O4	
1×	178.2(7)	As2–O5	
1×	184.3(7)	As2–O6	
$[(\text{Cl}1)\text{Y}_4\text{As}_4]^{23+}$ polyhedron			
2×	325.1(1)	Cl1···Y3	
2×	330.3(1)	Cl1···Y3'	
2×	332.2(1)	Cl1···As1	
2×	334.5(1)	Cl1···As2	
$[(\text{Cl}2)\text{Y}_2\text{As}_4]^{17+}$ polyhedron			
1×	269.5(4)	Cl2–Y3	
1×	273.9(3)	Cl2–Y3'	
1×	348.9(4)	Cl2···As1	
1×	355.9(4)	Cl2···As1'	
1×	353.3(4)	Cl2···As2	
1×	357.5(4)	Cl2···As2'	

Table 8. Motifs of mutual adjunction for the $Y_5Cl_3[AsO_3]_4$ structure.

	O1	O2	O3	O4	O5	O6	Cl1	Cl2	C.N.
Y1	2/1	0/0	0/0	2/1	2/1	2/1	0/0	0/0	8
Y2	1/1	2/2	2/2	1/1	1/1	1/1	0/0	0/0	8
Y3	0/0	1/1	1/1	0/0	1/1	1/1	$0 + \frac{2}{4} + 0 +$	2/2	6 + 2
As1	1/1	1/1	1/1	0/0	0/0	0/0	0/0	0/0	3
As2	0/0	0/0	0/0	1/1	1/1	1/1	0/0	0/0	3
C.N.	3	4	4	3	4	4	0 + 4	2	

3.3. Luminescence of Eu^{3+} - and Tb^{3+} -Doped Samples

None of the samples exhibits a luminescence under a UV lamp of 254 and 366 nm visible by the naked eye. This is presumably due to the low doping degree of about 0.6%. The effect of the low doping concentration can especially be seen in the spectra of $Y_5X_3[AsO_3]_4:Tb^{3+}$ (Figure 12b,d). Besides the normally recorded $^5D_4 \rightarrow ^7F_J$ ($J = 3-6$) transitions in the range from 480 to 630 nm, also the transitions $^5D_3 \rightarrow ^7F_J$ ($J = 3-6$) between 370 and 470 nm can be observed, adding a blue hue to the otherwise green emission. These energetically higher transitions are more intense the further away the Tb^{3+} cations are from adjacent ones, since the cross relaxation $^5D_3 \rightarrow ^5D_4$ with simultaneous excitation of a neighbouring Tb^{3+} particle from 7F_6 to excited 7F_J levels is less probable than [24]. A certain difference can be observed for the terbium-doped influence into the yttrium fluoride and chloride hosts. For $X = Cl$ the transitions from the 5D_3 state are significantly stronger than for the samples with $X = F$, which leads to the assumption that the doped cations are somewhat closer in the latter case.

The excitation spectra of the terbium-doped compounds display very weak $f-f$ transitions from the 7F_6 ground state between 300 and 380 nm and an intense broad band at about 235 and 260 nm originating from $f-d$ transitions. The energetic position of these transitions hint at a rather weak coordination of the surrounding halide and oxide anions [25]. The exact position of all transitions and those of a suitable doped reference are listed in Tables 9 and 10.

Table 9. The excitation wavelengths and the assigned transitions of $Y_5X_3[AsO_3]_4:Tb^{3+}$ ($X = Cl$ and F) and $Tb_2[B_2(SO_4)_6]$ as reference from [26].

	$Y_5Cl_3[AsO_3]_4:Tb^{3+}$	$Y_5F_3[AsO_3]_4:Tb^{3+}$	$Tb_2[B_2(SO_4)_6]$
Transition exc.	Wavelength/nm	Wavelength/nm	Wavelength/nm
$f-d$	233, 258	237, 262	212, 253
$^7F_6 \rightarrow ^5H_6$	–	304	301
$^7F_6 \rightarrow ^5H_7$	–	317	316
$^7F_6 \rightarrow ^5L_7, ^5L_8$	–	341	339
$^7F_6 \rightarrow ^5G_5$	–	351	356
$^7F_6 \rightarrow ^5L_{10}$	–	371	366
$^7F_6 \rightarrow ^5G_6$	–	377	373

The spectra of the europium-doped compounds (Figure 12a,c) exhibit similar features as the previously discussed terbium spectra. The transitions from the energetically higher 5D_1 state to 7F_J ($J = 1, 2$) in the regime from 530 to 560 nm are weakly present as well as the $^5D_0 \rightarrow ^7F_J$ ($J = 1-4$) transitions between 580 and 710 nm. The hypersensitive $^5D_0 \rightarrow ^7F_2$ electric dipolar transition is stronger than the $^5D_0 \rightarrow ^7F_1$ magnetic dipolar transition, which is caused by the absence of inversion symmetry at the doped sites. This is in accordance with the site symmetry of the yttrium atoms' Wyckoff positions (Tables 2 and 6).

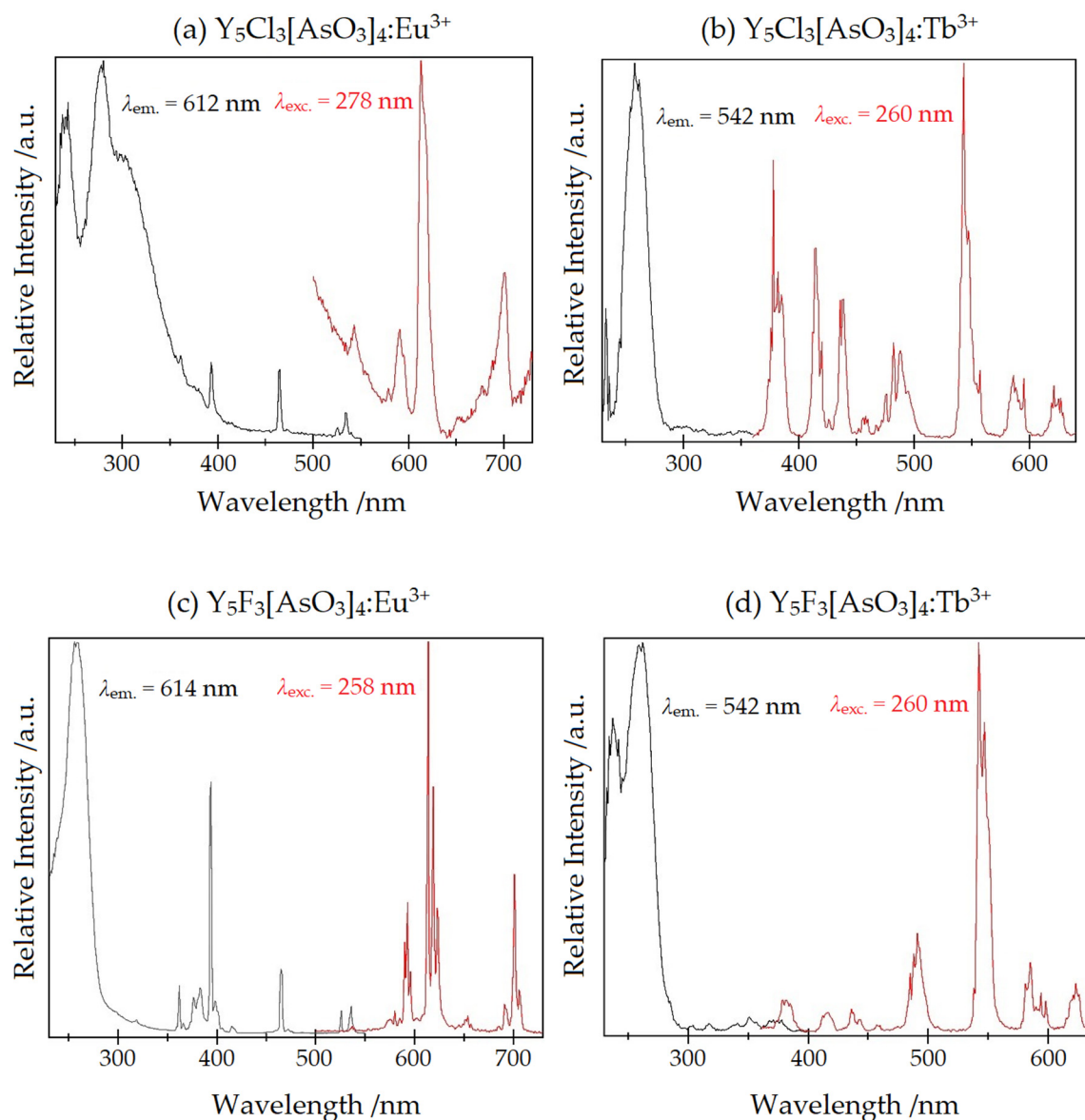


Figure 12. The luminescence spectra of (a) $\text{Y}_5\text{Cl}_3[\text{AsO}_3]_4:\text{Eu}^{3+}$, (b) $\text{Y}_5\text{Cl}_3[\text{AsO}_3]_4:\text{Tb}^{3+}$, (c) $\text{Y}_5\text{F}_3[\text{AsO}_3]_4:\text{Eu}^{3+}$ and (d) $\text{Y}_5\text{F}_3[\text{AsO}_3]_4:\text{Tb}^{3+}$. The emission spectra are displayed in red and those for excitation in black.

Table 10. The emission wavelengths and the assigned transitions of $\text{Y}_5\text{X}_3[\text{AsO}_3]_4:\text{Tb}$ ($\text{X} = \text{Cl}$ and F) and $\text{Y}_{1.998}\text{Tb}_{0.002}[\text{B}_2(\text{SO}_4)_6]$ as reference from [26].

	$\text{Y}_5\text{Cl}_3[\text{AsO}_3]_4:\text{Tb}^{3+}$	$\text{Y}_5\text{F}_3[\text{AsO}_3]_4:\text{Tb}^{3+}$	$\text{Y}_2[\text{B}_2(\text{SO}_4)_6]:\text{Tb}^{3+}$
Transition em.	Wavelength/nm	Wavelength/nm	Wavelength/nm
$^5\text{D}_3 \rightarrow ^7\text{F}_6$	378, 382, 385	382	—
$^5\text{D}_3 \rightarrow ^7\text{F}_5$	415, 420	417	411
$^5\text{D}_3 \rightarrow ^7\text{F}_4$	436, 439	437, 443	434
$^5\text{D}_3 \rightarrow ^7\text{F}_3$	456, 458, 460	—	—
$^5\text{D}_4 \rightarrow ^7\text{F}_6$	482, 488	491	490
$^5\text{D}_4 \rightarrow ^7\text{F}_5$	543, 547, 557	542, 547	541
$^5\text{D}_4 \rightarrow ^7\text{F}_4$	586, 595	585, 594, 598	583, 588
$^5\text{D}_4 \rightarrow ^7\text{F}_3$	621, 627	623	617, 621

The excitation spectra display $f-f$ transitions from the 7F_0 ground state between 350 and 530 nm. The excitation at 535 nm is due to the ${}^7F_1 \rightarrow {}^5D_1$ transition. Additionally, a broad charge-transfer band (CT) of europium around 260 nm occurs. For $X = \text{Cl}$ this charge transfer is split up into three peaks, possibly because of the varied surrounding at the different yttrium sites. For $[\text{EuCl}_6]^{3-}$ in acetonitril the charge-transfer band is reported at 301 nm and for $[\text{Eu}(\text{SO}_4)]^+$ at 240 nm [27], which falls into the same range as the measured ones. A compilation of the exact positions for all transitions and these of a reference can be found in Tables 11 and 12.

Table 11. The excitation wavelengths and the assigned transitions of $\text{Y}_5\text{X}_3[\text{AsO}_3]_4:\text{Eu}^{3+}$ ($X = \text{Cl}$ and F) and $\text{Eu}_2[\text{B}_2(\text{SO}_4)_6]$ as reference from [26].

	$\text{Y}_5\text{Cl}_3[\text{AsO}_3]_4:\text{Eu}^{3+}$	$\text{Y}_5\text{F}_3[\text{AsO}_3]_4:\text{Eu}^{3+}$	$\text{Eu}_2[\text{B}_2(\text{SO}_4)_6]$
Transition exc.	Wavelength/nm	Wavelength/nm	Wavelength/nm
CT	243, 278	258	265
${}^7F_0 \rightarrow {}^5H_{4-7}$	–	319	316
${}^7F_0 \rightarrow {}^5D_4$	361	362	360
${}^7F_0 \rightarrow {}^5G_{3-6}$	–	376	374
${}^7F_0 \rightarrow {}^5G_2$	–	384	381
${}^7F_0 \rightarrow {}^5L_6$	393	394	392
${}^7F_1 \rightarrow {}^5D_3$	–	415	412
${}^7F_0 \rightarrow {}^5D_2$	464	465	–
${}^7F_0 \rightarrow {}^5D_1$	526	526	–
${}^7F_1 \rightarrow {}^5D_1$	535	536	–

Table 12. The emission wavelengths and the assigned transitions of $\text{Y}_5\text{X}_3[\text{AsO}_3]_4:\text{Eu}^{3+}$ ($X = \text{Cl}$ and F) and $\text{Eu}_2[\text{B}_2(\text{SO}_4)_6]$ as reference from [26].

	$\text{Y}_5\text{Cl}_3[\text{AsO}_3]_4:\text{Eu}^{3+}$	$\text{Y}_5\text{F}_3[\text{AsO}_3]_4:\text{Eu}^{3+}$	$\text{Eu}_2[\text{B}_2(\text{SO}_4)_6]$
Transition em.	Wavelength/nm	Wavelength/nm	Wavelength/nm
${}^5D_1 \rightarrow {}^7F_0$	–	510	–
${}^5D_1 \rightarrow {}^7F_1$	–	538	–
${}^5D_1 \rightarrow {}^7F_2$	–	554, 558	–
${}^5D_0 \rightarrow {}^7F_1$	587	590, 593	585, 591, 595
${}^5D_0 \rightarrow {}^7F_2$	613, 618	614, 619, 623	610, 615, 621
${}^5D_0 \rightarrow {}^7F_3$	–	651, 654	647, 650, 653
${}^5D_0 \rightarrow {}^7F_4$	703	691, 701, 706	690, 697

In contrast to the antimony compounds $\text{YSb}_2\text{O}_4\text{X}$ ($X = \text{Cl}$ and Br) [14], where the lone pair at the Sb^{3+} cations contributes to the relevant energy-transfer processes, no such participation of the lone pair at the As^{3+} cations could be detected for the here investigated $\text{Y}_5\text{X}_3[\text{AsO}_3]_4:\text{Eu}^{3+}$ or $\text{Y}_5\text{X}_3[\text{AsO}_3]_4:\text{Tb}^{3+}$ samples with $X = \text{F}$ and Cl.

3.4. Conclusions and Outlook

With $\text{Y}_5\text{F}_3[\text{AsO}_3]_4$ and $\text{Y}_5\text{Cl}_3[\text{AsO}_3]_4$, two new compounds were obtained that have absolutely the same composition apart from the halogen, but very different crystal structures. It would be very interesting to find out, whether the structures with the heavy halides bromide ($\text{Y}_5\text{Br}_3[\text{AsO}_3]_4$) and iodide ($\text{Y}_5\text{I}_3[\text{AsO}_3]_4$) are also different or if they follow the new structure type of the chloride $\text{Y}_5\text{Cl}_3[\text{AsO}_3]_4$ or the lanthanoid(III) bromide derivatives $\text{Ln}_5\text{Br}_3[\text{AsO}_3]_4$ [28,29]. Moreover, luminescence measurements were carried out for undoped samples and those doped with Eu^{3+} and Tb^{3+} for both $\text{Y}_5\text{F}_3[\text{AsO}_3]_4$ and $\text{Y}_5\text{Cl}_3[\text{AsO}_3]_4$.

Author Contributions: Conceptualization, R.J.C.L. and T.S.; methodology, R.J.C.L., M.M., F.L., F.C.Z., H.A.H. and T.S.; software, R.J.C.L. and M.M.; validation, R.J.C.L. and M.M.; formal analysis, R.J.C.L. and M.M.; investigation, R.J.C.L. and M.M.; resources, H.A.H. and T.S.; data curation, R.J.C.L. and M.M.; writing—original draft preparation, R.J.C.L., M.M., T.S. and H.A.H.; writing—review and editing, T.S. and H.A.H.; visualization, R.J.C.L. and M.M.; supervision, T.S. and H.A.H.; project administration, T.S. and H.A.H.; funding acquisition, T.S. and H.A.H. All authors have read and agreed to the published version of the manuscript.

Funding: This research received no external funding.

Data Availability Statement: Data are available from the authors upon request.

Acknowledgments: The authors thank Falk Lissner for the single-crystal X-ray diffraction measurements.

Conflicts of Interest: The authors declare no conflicts of interest.

References

1. Shannon, R.D. Revised Effective Ionic Radii and Systematic Studies of Interatomic Distances in Halides and Chalcogenides. *Acta Crystallogr.* **1975**, *A32*, 751–767. [[CrossRef](#)]
2. Brauer, G.; Gradinger, H. Über heterotype Mischphasen bei Seltenerdoxyden I. *Z. Anorg. Allg. Chem.* **1954**, *276*, 209–226. [[CrossRef](#)]
3. Zalkin, A.; Templeton, D.H. The crystal structure of YF_3 and related compounds. *J. Am. Chem. Soc.* **1953**, *75*, 2453–2458. [[CrossRef](#)]
4. Hund, F. Yttriumoxyfluorid. *Z. Anorg. Allg. Chem.* **1951**, *265*, 62–66. [[CrossRef](#)]
5. Meyer, G.; Staffel, T. Die Tieftemperatur-Synthese von Oxidhalogeniden, YOX ($X = \text{Cl, Br, I}$), als Quelle der Verunreinigung von Yttriumtrihalogeniden, YX_3 , bei der Gewinnung nach der Ammoniumhalogenid-Methode. Die Analogie von YOCl und YsCl . *Z. Anorg. Allg. Chem.* **1986**, *532*, 31–36. [[CrossRef](#)]
6. Drafall, L.E.; McCarthy, G.J.; Sipe, C.A.; White, W.B. On the preparation and X-ray powder data of rare earth sulfides and oxysulfides. *Proc. Rare-Earth Res. Conf.* **1974**, *2*, 954–959.
7. Schleid, T.; Strobel, S.; Dorhout, P.K.; Nockemann, P.; Binnemans, K.; Hartenbach, I. $\text{YF}[\text{MoO}_4]$ and $\text{YCl}[\text{MoO}_4]$: Two halide derivatives of yttrium *ortho*-oxomolybdate: Syntheses, structures, and luminescence properties. *Inorg. Chem.* **2008**, *47*, 3728–3735. [[CrossRef](#)]
8. Schustereit, T. Synthese und Charakterisierung Anionischer Derivate von Seltenerdmetall-Oxidomolybdaten und -Wolframaten mit Hilfe Festkörper- und Nasschemischer Methoden. Ph.D. Thesis, University of Stuttgart, Stuttgart, Germany, 2015.
9. Lipp, C.; Schleid, T. A new rare-earth metal(III) fluoride oxoselenate(IV): $\text{YF}[\text{SeO}_3]$. *Z. Anorg. Allg. Chem.* **2008**, *634*, 657–661. [[CrossRef](#)]
10. Chou, S.-C.; Greiner, S.; Magdysyuk, O.V.; Dinnebier, R.E.; Schleid, T. Theoretical and experimental analysis of structural phase transitions for $\text{ScF}[\text{SeO}_3]$ and $\text{YF}[\text{SeO}_3]$. *Z. Anorg. Allg. Chem.* **2014**, *640*, 3203–3211. [[CrossRef](#)]
11. Li, P.-F.; Hu, C.-L.; Kong, F.; Mao, J.-G. The first UV nonlinear optical selenite material. Fluorination control in $\text{CaYF}(\text{SeO}_3)_2$ and $\text{Y}_3\text{F}(\text{SeO}_3)_4$. *Angew. Chem. Int. Ed.* **2023**, *62*, e202301420. [[CrossRef](#)]
12. Schleid, T.; Hartenbach, I. On halide derivatives of rare-earth metal(III) oxidomolybdates(VI) and -tungstates(VI). *Z. Kristallogr.* **2016**, *231*, 449–466. [[CrossRef](#)]
13. Schustereit, T.; Netzsch, P.; Höpfe, H.A.; Hartenbach, I. Green light. On $\text{YCl}[\text{WO}_4]$ as host material for luminescence active Tb^{3+} cations. *Z. Anorg. Allg. Chem.* **2018**, *644*, 1749–1753. [[CrossRef](#)]
14. Locke, R.J.C.; Goerigk, F.C.; Schäfer, M.J.; Höpfe, H.A.; Schleid, T. Synthesis, crystal structures and spectroscopic properties of pure $\text{YSb}_2\text{O}_4\text{Br}$ and $\text{YSb}_2\text{O}_4\text{Cl}$ as well as Eu^{3+} - and Tb^{3+} -doped samples. *Roy. Soc. Chem. Adv.* **2022**, *12*, 640–647. [[CrossRef](#)] [[PubMed](#)]
15. Herrendorf, W.; Bärnighausen, H. *HABITUS: Program for the Optimization of the Crystal Shape for Numerical Absorption Correction in X-SHAPE, version 1.06*; Fa. Stoe: Darmstadt, Germany, 1996.
16. Sheldrick, G.M. *SHELXS-97 and SHELXL-97: Programs for Solution and Refinement of Crystal Structures from X-Ray Diffraction Data*; University of Göttingen: Göttingen, Germany, 1997.
17. Locke, R.J.C.; Ledderboge, F.; Goerigk, F.C.; Zimmer, F.C.; Schleid, T. The isotypic series of tetragonal lanthanoid(III) fluoride oxoarsenates(III) $\text{Ln}_5\text{F}_3[\text{AsO}_3]_4$ ($\text{Ln} = \text{Eu-Lu}$). *Z. Naturforsch.* **2024**, *79b*, 357–367. [[CrossRef](#)]
18. Bevan, D.J.M.; Mann, A.W. The crystal structure of $\text{Y}_7\text{O}_6\text{F}_9$. *Acta Crystallogr.* **1975**, *B31*, 1406–1411. [[CrossRef](#)]
19. Bevan, D.J.M.; Mohyla, J.; Hoskins, B.F.; Steen, R.J. The crystal structures of some Vernier phases in the yttrium oxide-fluoride system. *Eur. J. Solid State Inorg. Chem.* **1990**, *27*, 451–465.

20. Pertlik, F. Verfeinerung der Kristallstruktur des Minerals Claudetit, As_2O_3 (Claudetit I). *Monatsh. Chem. Chem. Monthly* **1978**, *109*, 277–282. [[CrossRef](#)]
21. Pertlik, F. Die Kristallstruktur der monoklinen Form von As_2O_3 (Claudetit II). *Monatsh. Chem. Chem. Monthly* **1975**, *106*, 755–762. [[CrossRef](#)]
22. Pertlik, F. Structure refinement of cubic As_2O_3 (arsenolite) with single crystal data. *Czech. J. Phys.* **1978**, *B28*, 170–176. [[CrossRef](#)]
23. Goerigk, F.C.; Schander, S.; Ben Hamida, M.; Kang, D.-H.; Ledderboge, F.; Wickleder, M.S.; Schleid, T. Die monoklinen Seltenerdmetall(III)-Chlorid-Oxidoarsenate(III) mit der Zusammensetzung $\text{SE}_5\text{Cl}_3[\text{AsO}_3]_4$ ($\text{SE} = \text{La} - \text{Nd}, \text{Sm}$). *Z. Naturforsch.* **2019**, *74b*, 497–506. [[CrossRef](#)]
24. Höpfe, H.A. *Rare-Earth Elements*, 1st ed.; de Gruyter: Berlin, Germany, 2024.
25. Netzsch, P.; Bariss, H.; Bayarjargal, L.; Höpfe, H.A. $\text{Tb}(\text{HSO}_4)(\text{SO}_4)$ —A green emitting hydrogensulfate sulfate with second harmonic generation response. *Dalton Trans.* **2019**, *48*, 16377–16383. [[CrossRef](#)] [[PubMed](#)]
26. Netzsch, P.; Hämmer, M.; Gross, P.; Bariss, H.; Block, T.; Heletta, L.; Pöttgen, R.; Bruns, J.; Huppertz, H.; Höpfe, H.A. $\text{RE}_2[\text{B}_2(\text{SO}_4)_6]$ ($\text{RE} = \text{Y}, \text{La} - \text{Nd}, \text{Sm}, \text{Eu}, \text{Tb} - \text{Lu}$): A silicate-analogous host structure with weak coordination behaviour. *Dalton Trans.* **2019**, *48*, 4387–4397. [[CrossRef](#)] [[PubMed](#)]
27. Binnemans, K. Interpretation of europium(III) spectra. *Coord. Chem. Rev.* **2015**, *295*, 1–45. [[CrossRef](#)]
28. Locke, R.J.C.; Ledderboge, F.; Goerigk, F.C.; Zimmer, F.C.; Schleid, T. About the Rare-Earth Metal(III) Bromide Oxoarsenates(III) $\text{RE}_5\text{Br}_3[\text{AsO}_3]_4$ with A- ($\text{RE} = \text{La}$ and Ce) or B-Type Structure ($\text{RE} = \text{Pr}, \text{Nd}, \text{Sm} - \text{Tb}$) and $\text{RE}_3\text{Br}_2[\text{AsO}_3][\text{As}_2\text{O}_5]$ ($\text{RE} = \text{Y}, \text{Dy} - \text{Yb}$). *Solids* **2025**, *6*, 4. [[CrossRef](#)]
29. Locke, R.J.C. Synthese und Charakterisierung von Seltenerdmetall-Halogenid-Oxoarsenaten(III) und -Oxoantimonaten(III) mit Ausläufern zu den entsprechenden -Oxobismutaten(III). Ph.D. Thesis, University of Stuttgart, Stuttgart, Germany, 2025.

Disclaimer/Publisher’s Note: The statements, opinions and data contained in all publications are solely those of the individual author(s) and contributor(s) and not of MDPI and/or the editor(s). MDPI and/or the editor(s) disclaim responsibility for any injury to people or property resulting from any ideas, methods, instructions or products referred to in the content.